Space Imaging Geodesy Reveals Near Circular, Coseismic Block Rotation During the 2016 Mw 7.8 Kaikōura Earthquake, New Zealand

Teng Wang, Liqing Jiao, Paul Tapponnier, Xuhua Shi, Shengji Wei

Geophysical Research Letters

RESEARCH LETTER
10.1029/2020GL090206

Key Points:
- Space imaging geodesy reveals coseismic block rotation during the 2016 Kaikōura earthquake
- Analytical and numerical modeling account for geodetic and local paleomagnetic evidence of clockwise rotation
- Block-rotation might have prevented rupturing on the Hope fault during the 2016 Kaikōura earthquake

Supporting Information:
- Supporting Information S1
- Movie S1
- Movie S2
- Movie S3

Correspondence to:
T. Wang,
wang.teng@pku.edu.cn

Citation:
Wang, T., Jiao, L., Tapponnier, P., Shi, X., & Wei, S. (2020). Space imaging geodesy reveals near circular, coseismic block rotation during the 2016 M_w 7.8 Kaikōura earthquake, New Zealand. *Geophysical Research Letters*, *47*, e2020GL090206. https://doi.org/10.1029/2020GL090206

Received 11 AUG 2020
Accepted 5 NOV 2020
Accepted article online 9 NOV 2020

Space Imaging Geodesy Reveals Near Circular, Coseismic Block Rotation During the 2016 M_w 7.8 Kaikōura Earthquake, New Zealand

Teng Wang[1], Liqing Jiao[2], Paul Tapponnier[3], Xuhua Shi[4,5], and Shengji Wei[6]

[1]School of Earth and Space Sciences, Peking University, Beijing, China, [2]Institut de Physique du Globe de Paris, CNRS, Université de Paris, Paris, France, [3]Key Laboratory of Crustal Dynamics, National Institute of Natural Hazards, MEMC, Beijing, China, [4]School of Earth Sciences, Zhejiang University, Hangzhou, China, [5]Research Center for Structures in Oil- and Gas-Bearing Basins, Ministry of Education, Hangzhou, China, [6]Earth Observatory of Singapore/Asian School of the Environment, Nanyang Technological University, Singapore, Singapore

Abstract Large earthquakes usually rupture plate boundary faults, releasing the accumulated stress as displacements localized along smooth, narrow faults. However, certain earthquakes initiate off main faults, rupturing adjacent, secondary faults. The mechanisms of such atypical stress release remain enigmatic, partly due to a lack of detailed geodetic evidence. Here using the 3D coseismic displacement field derived from space imaging geodesy, we detect 10-km-scale, nearly-circular coseismic block rotation during the 2016 M_w 7.8 Kaikōura earthquake in New Zealand. Together, geodetic observations, longer term local paleomagnetic data, analytical, and discrete element modeling imply that localized block rotation occurred south of the Hope fault along weak, steep, bedding-parallel boundaries within a narrow, ~20-km-wide dextral shear zone. That stress near plate boundary faults can be partially released in zones of distributed ruptures absorbing coseismic rotation may retard rupture along main faults. Our observations also suggest that coseismic rotation may help accomodate plate boundary propagation.

Plain Language Summary That the M_w 7.8, 2016, Kaikōura (New Zealand) earthquake, whose epicenter was near the Hope fault, did not rupture that fault which accommodates over half of the ~40 mm/year Pacific/Australian plate motion, is puzzling. Space-borne radar images, that reveal fine details of the displacements within a 100-km-long and ~20-km-wide area south the Hope fault, show a clear pattern of clockwise block rotation bounded by three near-orthogonal surface ruptures. Coseismic slips along the northern and southern edges of the block were ~2 m, a total close to the 5-m slip accumulated since ~AD 1780 on the Hope fault. Crustal block rotation thus played a significant role in releasing accumulated strain, possibly preventing farther rupture propagation along that fault. Our geodetic observations and numerical modeling are in keeping with longer timescale paleomagnetic rotation along the same crustal shear zone, confirming the tight link between large seismic events and the broader tectonic regime.

1. Introduction

Along coupled plate boundaries, stress is built up and recurrently released during earthquakes as displacement, strain, and rotation (Segall, 2010). Coseismic displacement and strain have been well observed and modeled, but coseismic, kilometer-scale, block rotation has not yet been unambiguously captured. Although orientations of geological features, paleomagnetic measurements, and earthquake focal mechanisms have provided clues about crustal rotation, particularly along transform or transfer zones, for instance, in Afar (Tapponnier et al., 1990), Iceland (Green et al., 2013; Horst et al., 2018), and New Zealand (Hall et al., 2004; Randall et al., 2011; Wallace, 2004), the lack of direct observation of rotation during an earthquake impedes our understanding of its occurrence and role in the earthquake cycle.

New Zealand straddles the Australia-Pacific plate boundary, with the dextral strike-slip Alpine Fault connecting the west-dipping Hikurangi subduction zone in the north to the east-dipping Puysegur subduction in the south (Figure 1, inset). Between the Hikurangi trench and the Alpine Fault, an ~150-km-wide belt of active dextral strike-slip faults, the Marlborough Fault Zone (MFZ), cumulatively accommodates most of the ~38 mm/year relative plate motion (e.g., Hall et al., 2004; Little & Jones, 1998; Randall et al., 2011; Wallace et al., 2012; Wannamaker et al., 2009). The four major faults of the MFZ (the Alpine-Wairau,

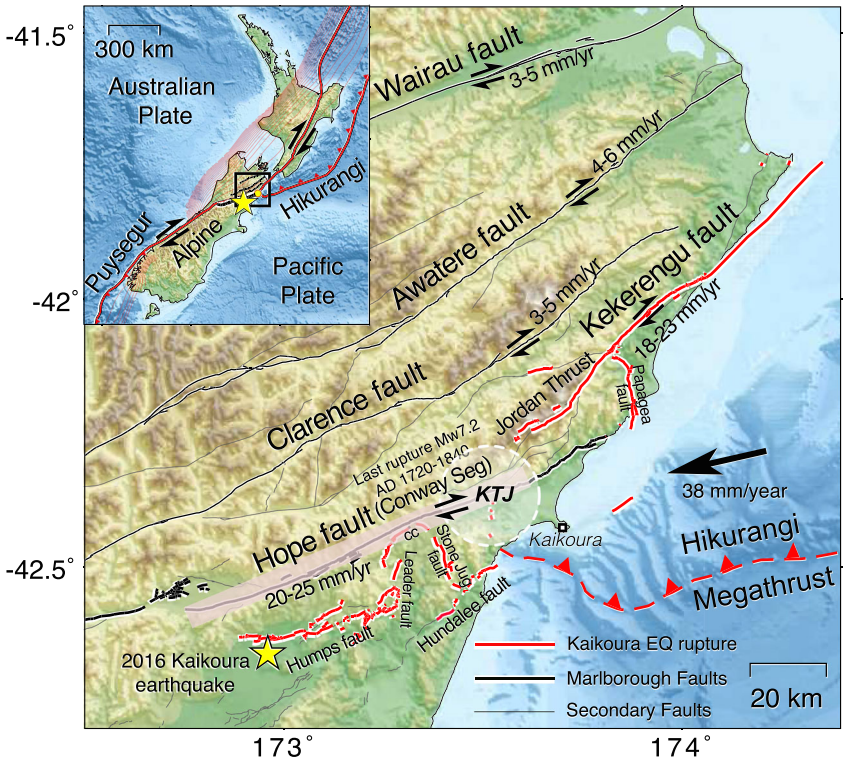

Figure 1. Tectonic setting of the Marlborough Fault Zone showing all active faults (Litchfield et al., 2013) and 2016 Kaikōura earthquake ruptures (Nicol et al., 2018; Stirling et al., 2017). The inset shows the simplified plate boundary zone across New Zealand. The large black arrow indicates the relative motion between the Pacific and Australian Plates (Argus & Gordon, 1991). The Marlborough fault system includes four major right-lateral strike-slip faults, with Holocene, slip rates $\lesssim \approx 5$ millimeter (Little et al., 2018; Mason et al., 2006; Zachariasen et al., 2006). From paleo-seismological trenching, the last earthquake that ruptured the Conway Segment of the Hope fault west of Kaikōura occurred between 1720 and 1840 (Langridge et al., 2003), ~15 km north of the 2016 epicenter (yellow star). Red lines are 2016 surface ruptures from Nicol et al. (2018), and CC is the Conway-Charwell fault. Dashed red line with teeth is inferred western extension of Hikurangi subduction boundary. KTJ and dashed white circle indicate inferred position of Kaikōura Triple Junction (Shi et al., 2019).

Awatere, Clarence, and Hope-Kekerengu faults) lie ~30 km apart and appear to become younger southwards (e.g., Little & Jones, 1998), (Figure 1). This is consistent with a southwestward propagation of the Hikurangi subduction zone (e.g., Shi et al., 2019; Wallace et al., 2012; Wannamaker et al., 2009). The southernmost fault, the Hope fault, slips at a rate of 20–25 mm/year, accommodating at least half of the plate motion (e.g., Langridge et al., 2003; Little et al., 2018; Vandissen & Yeats, 1991). Paleo-seismological studies along the eastern Hope fault indicate that the latest large earthquake (M_w ~ 7.2) ruptured the fault in AD 1780 ± 60 (Langridge et al., 2003) (Figure 1). Given the 20–25 mm/year interseismic slip rate, about 5 m of displacement deficit had thus built up along the fault before the 2016 Kaikōura earthquake.

The rupture of the November 2016 Kaikōura earthquake initiated at shallow depth on the Humps fault, ~15 km south of the Hope fault (Figure 1), and propagated towards the northeast, involving as many as 17 shallow crustal faults (e.g., Cesca et al., 2017; Clark et al., 2017; Hamling et al., 2017; Wang et al., 2018). We mapped the surface coseismic displacement using Synthetic Aperture Radar (SAR) images acquired by the Sentinel-1 and ALOS-2 satellites and inverted for the 3D displacements on designed grids (Wang et al., 2018) (Supporting Information S1). In keeping with field investigations (Nicol et al., 2018) and other geodetic imaging studies (e.g., Hamling et al., 2017; Morishita et al., 2017; Xu et al., 2018; Zinke et al., 2019), no coseismic displacement discontinuity was observed across the Hope fault. Instead, the Kaikōura earthquake activated several faults within a 100-km-long and 20-km-wide zone of crustal slivers between the Hope fault and the Humps-Leader/Hundalee faults (Nicol et al., 2018) (Figure 1). Surface displacements

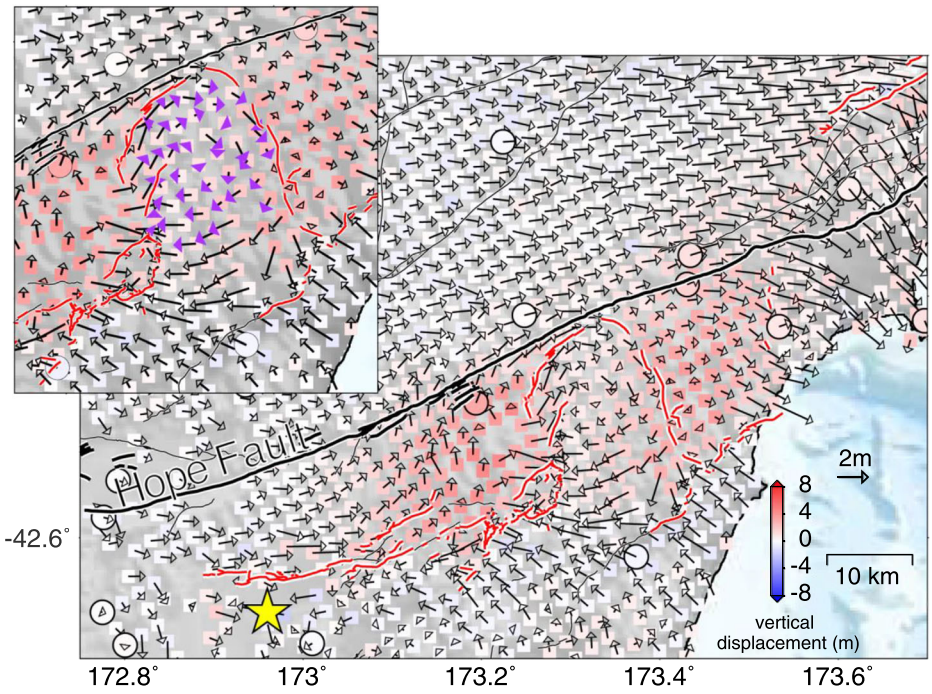

Figure 2. Three-dimensional (3D) coseismic displacements along the Hope fault. The displacements are derived from GPS (circles), Sentinel-1, and ALOS-2 SAR images (squares), with arrows showing horizontal and colors showing vertical displacements. Red lines are 2016 surface fault ruptures as in Figure 1. Top-left inset shows enlarged field displaying clear coseismic clockwise rotation pattern (enhanced violet arrows).

included 1.6 m of right-lateral slip on the Conway-Charwell fault, ~1 km south of the Hope fault, and 0.5–1.5 m of lateral slip on several previously unmapped faults (e.g., Leader and Stone Jug faults), roughly perpendicular to the Hope fault (Nicol et al., 2018; Zinke et al., 2019) (Figure 1). To better assess the coseismic deformation distribution within this zone, we calculated the 3D displacements on finer grid cells (2 × 2 km) aligned along the Hope fault (Figure 2).

2. Geodetic Rotation Observations and Modeling

A clear pattern of clockwise rotation emerges from our results, particularly in the inner part of the middle sliver (Figure 2, inset). Based on the finite-fault (FF) slip model derived from seismic and geodetic data (Wang et al., 2018), we improve the inversion by adjusting the locations and dip-angles of the three shallow faults (Leader, Stone Jug, and Conway-Charwell faults) that bound this sliver, following the latest surface rupture map (Nicol et al., 2018) and local geological map (Rattenbury et al., 2006) (Figure S1). Our updated FF model roughly reproduces a pattern of clockwise rotation, but it fails to reproduce the large westward spin along the southwest boundary of the block (Figures 3b and 3d). By contrast, most of the coseismic horizontal motions may be best fitted by a 0.008° clockwise rotation around a vertical axis (Figures 3a and 3c and Supporting Information S1). The fit of this simple rotation model has RMS residuals (0.51 m in the west-east and 0.38 m in the south-north directions) comparable to those of the FF model (0.46 m in the west-east and 0.33 m in the south-north directions). The clearest discrepancies between the two models are observed along the western-boundary (Leader fault) and along the southern, un-faulted edge of the block (Figures 3c, 3d, and S2–S3).

Assuming a purely rigid block rotation, the radial strain to the rotating pole should be zero everywhere within the block. Our observations do show smaller radial strains than the elastic model predicts in the inner part of the block (Figure S3). The rigid block model also shows smaller misfits in the areas away from surface ruptures, such as the southwest part of the block, but larger misfits along the ruptured faults than the FF model (Figures 3 and S2). Thus, the surface deformation observed must be a combination of elastic strain

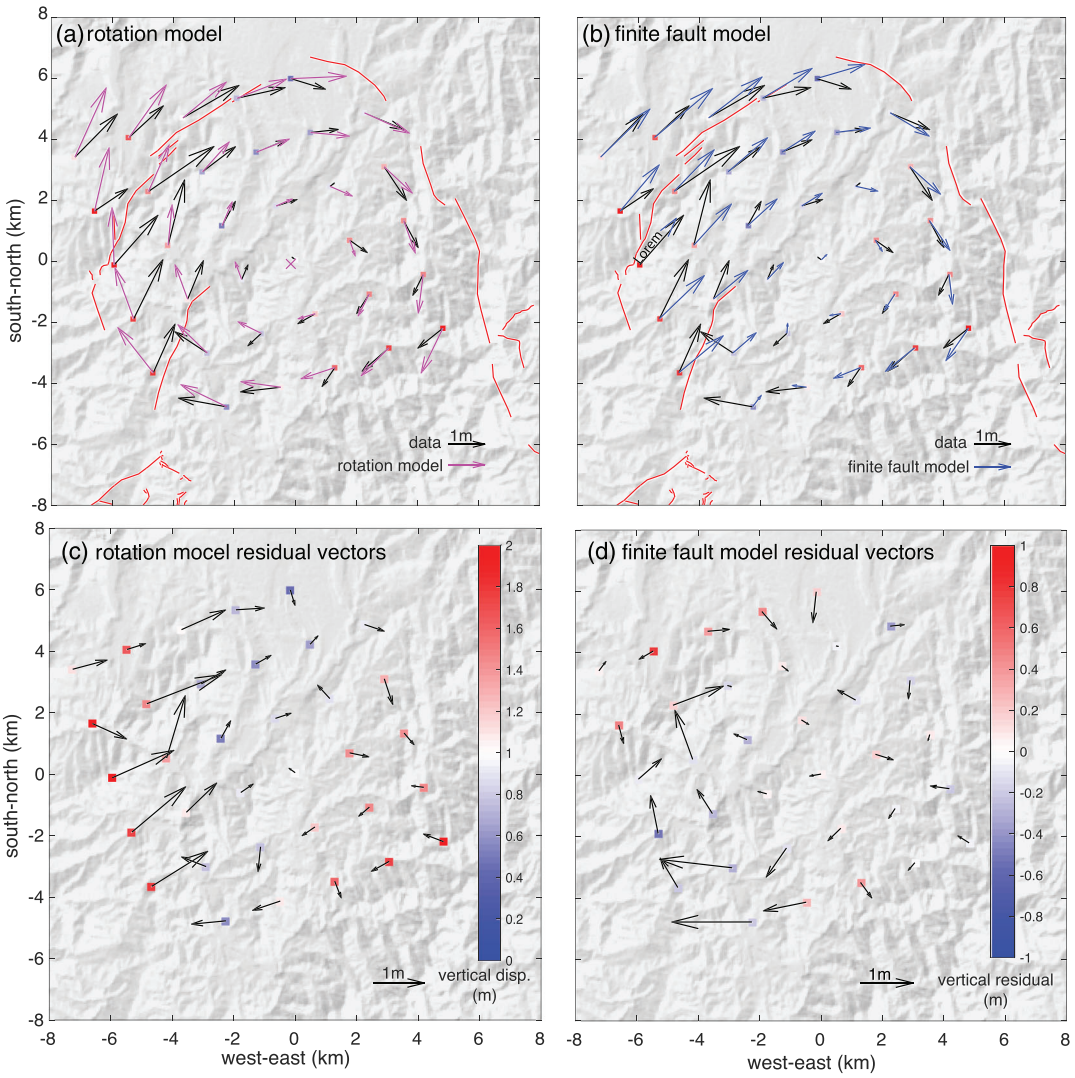

Figure 3. Fitting of the geodetic data. Selected central area of inset in Figure 2, with geodetic data (black arrows in a and b) showing roughly circular rotation pattern between approximately orthogonal 2016 surface ruptures (red lines). Plot (a) shows best-fitting predictions (purple arrows) from a simple rigid block rotation model (purple cross indicates derived vertical-axis rotation pole). Plot (b) shows best-fitting predictions (blue arrows) from finite-fault (FF) slip model based on teleseismic, strong-motion, and geodetic data. Plots (c) and (d) show corresponding residuals. Note that vertical displacements are not modeled in the block-rotation case. They are thus plotted with the same symbols (colored squares) in (a) and (c).

and rotation. The elastic deformation dominates near the faults that ruptured, while the rigid-block rotation is more obvious in the unfaulted part of the block. Nevertheless, the similarity between the block model and the FF model does show that, when faulting is distributed within a small area (e.g., within 20 × 20 km), the difference between block rotation and distributed deformation may be blurred (e.g., Thatcher, 2009).

With a rotation angle of 0.008°, the slips along the northern and southern edges of the block are ~2 m, the sum of which is 80% of the total 5-m slip deficit along this part of the Hope fault since AD 1780. The combination of strain and rotation thus appears to have released most of the shear stress accumulated across the ~20-km-wide shear zone during the ~240-year-long interseismic period, yet without rupturing the Hope fault. This, however, only concerns a short, 10-km-long segment of that Fault, which might act as a barrier for rupture, or as a short segment with much smaller slip at shallow depth, during the next large earthquake.

To further explore the mechanical conditions that might foster block rotation and to better understand the regional deformation and rupture complexity along and inside a long-term shear zone, we use a discrete

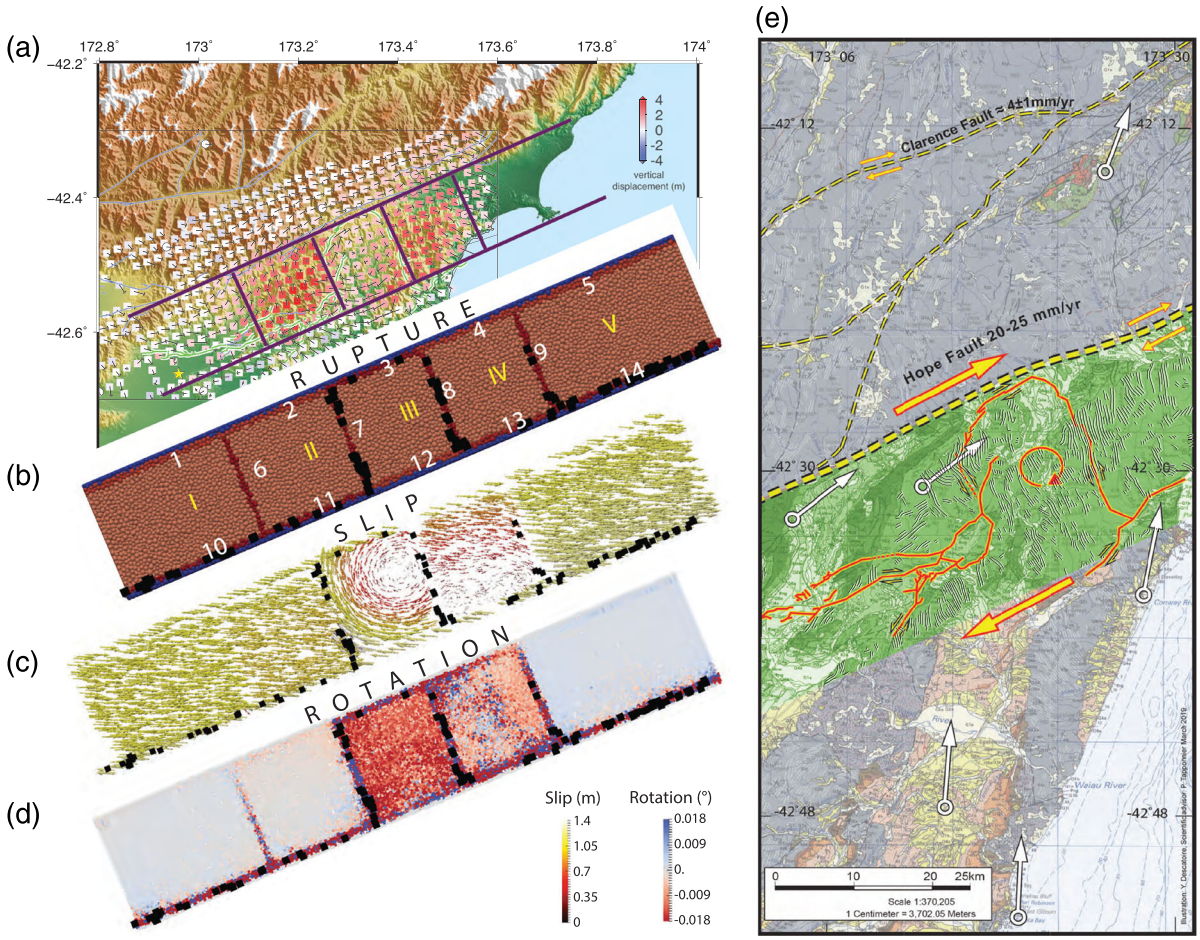

Figure 4. Simplified geological/tectonic setting of west Kaikōura shear zone and regional discrete element modeling. Plots (a) and (b) show ≈150-km-long, ≈25-km-wide shear zone location, boundaries, and model settings, with 5 distinct blocks (I to V), bounded by 14 weak zones 900 m-wide (1 to 14). Plots (c) and (d) show horizontal slip vectors and block rotations, during one rupture event. Amounts of slip and of clockwise/counter-clockwise rotations are color coded (bottom right). Black squares in (b)–(d) represent element bonds breakage (equivalent to fault ruptures). The total number of elements is 60,000 (see supporting information). Plot (e) shows the western part of 2016 earthquake surface ruptures (red lines from Stirling et al., 2017), superimposed on geologic map of north-eastern region of New Zealand's Southern Island (Rattenbury et al., 2006). Note that surface ruptures around east and west sides of rotating block follow steeply dipping Cretaceous beds (thin black lines; Rattenbury et al., 2006). Yellow dashed lines are principal active faults. Six white arrows are all local measurements of rotated paleomagnetic declination vectors in past 20 Ma (Randall et al., 2011). All rotation angles are clockwise relative to north. Red circular arrow indicates sense of block rotation. Width of green shaded shear zone, containing all faults seismically activated by 2016 event, is only ≈25 km. The largest paleomagnetic clockwise rotations (up to 40°) clearly express localized drag along the fastest slipping Hope fault (up to ~25 mm/year and ~60% of plate boundary motion), as commonly observed along large lithospheric shear zones.

element modeling approach in an elastoplastic crust (e.g., Jiao et al., 2018). In keeping with the simplified geometry of the 2016 surface ruptures, faulting during the Kaikōura earthquake is approximated to have occurred within a 20-km-wide, 100-km-long dextral shear zone containing rectangular fault-bounded blocks (Figures 4a and 4b). This technique enables rupture with relatively large displacements in tension, compression, shear, or mixed-mode boundary conditions (e.g., Jiao et al., 2018; Scholtes & Donze, 2013). Bonds between spherical elements break down when contact forces reach their limits (see supporting information). To promote faulting along the observed surface ruptures (Nicol et al., 2018), the strengths along the modeled block boundaries that ruptured during the earthquake were set to be ~100 times weaker than those inside the block interiors and 20 times weaker than the boundaries that did not rupture. The weak block boundaries must also be wide enough (≈0.9 km) to allow localized motion. While the width and strength of the boundary fault zones may affect the results, the fact that predominant, narrow rupture zones with large offsets are localized along the block edges does require that they be narrow and rheologically weak.

With an applied, persistent dextral shear, we ran such discrete element modeling to simulate 35 rupture events on the weak block boundary faults. Four out of these events produced nearly circular clockwise rotation patterns. That which best fit the observed geodetic rotations in Figure 3, produced an ~0.007–0.010° rotation of model block III (Figures 4c and 4d). The model derived rotation angle is similar to that derived from the SAR data using the simple rigid rotation in Figure 3a (0.008°). Note that block IV, farther northeast in the model, also rotates during this event, albeit less (~0.005–0.007°). The simulated event shows ~3 m of slip along the two main strike-slip boundary faults (Conway-Charwell faults to the north, and Humps-Leader-Hundalee faults to the south), with 1.5 m of convergence perpendicular to the Hope fault, both of which comparable to coseismic field and geodetic observations.

Given the preassigned, narrow weak zones, the variable stress conditions within the shear zone, and the different friction properties of the fault planes, the initiation and propagation of rupture should be expected to follow different paths during distinct seismic events. Quantitively investigating the preconditions controlling different rupture histories would thus be difficult, as the numerical models cannot simply account for all natural factors. Concerning the longer term deformation pattern, however, the discrete element modeling approach suggests that rotational events only happen occasionally, with somewhat different patterns, styles, and amounts. By contrast, most events (31 out of 35, i.e., nearly 90%) break only one or very few fault segments, as expected for earthquakes that rupture mostly the main boundary fault (see all 35 simulations in Supporting Information S1). Clearly, long-term geological records are required to investigate whether the simulated rupture-pattern variations occur or not in nature.

3. Large, Localized Paleomagnetic Rotations

Paleomagnetic declinations in Oligocene sediments just south of the Hope fault and northeast of the 2016 earthquake epicenter reveal large, coherent, and very localized clockwise rotations of ~40°, since about 20 Ma (Lamb, 2011; Randall et al., 2011), while much less perturbed declinations are observed north of the Hope Fault and south of the Hump Fault (Figure 4e). Farther to the northeast, within the broader Marlborough region, clockwise rotation appears to have occurred within large blocks at slower rates overall, except near the Awatere and Clarence faults (Randall et al., 2011). Yet farther east (figure 2 in Randall et al., 2011), maximum local rotations of up to 146° clockwise are documented just near the Kekerengu fault, while almost none are observed just south of it, east of the Papatea Fault (Figure 1).

Given the measured 2016 coseismic rotation of 0.008°, 5,000 large earthquakes comparable to the Kaikōura event would be required along the Hope-Humps shear zone to accrue 40° of finite clockwise rotation, at an average rate of 2°/Ma. Such earthquakes would recur every 4,000 years. That return time would be ~10 times longer than those derived from trenching along the Hope fault, under the simple assumption that large earthquakes on that fault occur regularly, in near-characteristic-slip fashion. Indeed, an average recurrence interval on the order of 400 years would be within the minimum and maximum Late Holocene return times estimated for large events along the Alpine-Hope fault (e.g., Berryman et al., 2012; Bull, 1996; Langridge et al., 2003). The recurrence time ratio between events with and without block rotation derived from geological data (paleomagnetic and trenching) would thus be roughly consistent with the ratio derived from discrete element model simulation (4 in 35 simulations). While this first-order, oversimplified comparison involves widely different timescales, it does suggest that the rupture complexity of the 2016 Kaikōura earthquake might be rare. The rarity of that event, which coinvolved kilometers-scale block rotation with surface slip along multiple, distinct faults with radically different strikes (including orthogonal) and senses of slip (right-lateral, left-lateral, and thrust), may be related to the mechanical difficulties of propagating coseismic rupture along two fast slipping (~20 to 25 mm/year) strike-slip faults (Hope and Kekerengu faults) that strike at an angle of as much as 24°, as well as across an FFT (Fault-Fault-Trench) type triple junction such as that with the Hikurangi megathrust near Kaikōura (Shi et al., 2019).

4. Discussion and Conclusions

Our geodetic observations and discrete element modeling suggest that coseismic block rotation may play an important role in releasing the interseismic stress accumulated between large earthquakes, by rupturing an array of secondary faults within a fairly narrow zone. It appears that both the distributed secondary faulting and the vertical-axis rotation were facilitated by the regional geological structure, which is characterized by

very steeply dipping (60°–80°) Cretaceous rocks with bedding-slip guiding faulting (Rattenbury et al., 2006) (Figure 4e). Instead of being driven by large-scale, regional tectonic motion, kilometer-scale rotations may be driven by localized dextral shear within narrow shear zones containing smaller, weak, preexisting faults. Interseismic motions on these faults were probably very slow (e.g., Lamb et al., 2018), essentially undetectable in the GPS-derived strain field, and not recognized before the Kaikōura earthquake.

The complexity of the 2016 Kaikōura earthquake suggests that distinguishing different rupture styles on faults with similar far-field slip rates determined from GPS data points may be very challenging. For example, within the region of highest macroseismic intensities (Cesca et al., 2017), both the Hope and Kekerengu faults show similar interseismic slip rates and evidence for surface rupture traces and offsets produced by large historical events (e.g., Little et al., 2018; Manighetti et al., 2015). However, only the Kekerengu fault ruptured in the 2016 event, showing localized slip of up to ~10 m along a smooth, ~60-km-long rupture trace. Note that this included nearly pure strike-slip along the Jordan Thrust (JDT), that actually also showed a small component of normal throw (Wang et al., 2018). On the other hand, west of the Kekerengu-JDT rupture, the Hope fault did not rupture, and coseismic deformation instead exhibited a completely different style, with block rotation and multiple ruptures on a complex array of different faults, some of which almost perpendicular to the Hope fault.

High-resolution geodetic and topographic/bathymetric imaging techniques reveal increasingly more rupture details along strike-slip faults. Such images show that rather than involving simple breaks localized on main faults, coseismic displacements are sometimes distributed within shear zones including parallel fault strands with radically different slip (e.g., 2001 Kokoxili earthquake: Fialko et al., 2005; King et al., 2005; Klinger et al., 2005), belts of damage zones (e.g., 2003 Bam earthquake: Fialko et al., 2005), conjugate strike-slip ruptures (e.g., 2012 Wharton-Basin earthquakes: Hill et al., 2015; Singh et al., 2017), and small-block rotations (this study). Slip promoting rotation on secondary faults in the uppermost part of the crust might provide a mechanism to account for the coseismic shallow slip deficit well observed during large strike-slip earthquakes (Fialko et al., 2005; Xu et al., 2016). Such complex rupture styles may depend on fault maturity (e.g., Perrin et al., 2016), or other factors including complexity in regional deformation kinematics.

Well-documented rotations often occur within transfer zones between rifts (e.g., Naar & Hey, 1991; Tapponnier et al., 1990), near the terminus of subduction zones (e.g., Wallace et al., 2012), or near plate triple junctions (e.g., Manighetti et al., 1998), attesting to the early stages of lateral migration/propagation of such junctions. To our knowledge, however, the data set shown and discussed here is the first to document approximately circular coseismic rotation at a scale of ~10 km in a region that can also be modeled quantitatively within a well-documented, continental, active faulting zone. Further high-resolution, geodetic measurements of coseismic rupture styles including localized rotations ought to be important to better understand crustal deformation mechanics and earthquake physics.

Data Availability Statement

The Sentinel-1A/B images are provided by the European Space Agency. The ALOS-2 images were provided by JAXA under the ALOS-2 RA4 Research Project 1413. The three-dimensional displacement data points used in this study can be downloaded online (https://disk.pku.edu.cn:443/link/DD387BCB17396FEA77ADCBA2F66A0813).

Acknowledgments

We thank Y. Descatoire and X. Zhang for preparing Figure 4 and Dr R. J. Weldon for constructive discussions at the early stage of this study. This work is funded by the National Key Research and Development Program of China (2019YFC1509204) and Natural Science Foundation of China (41974017, 41972227, and 41941016). Paul Tapponnier acknowledges a research grant (ZDJ2019-19) from the Institute of Crustal Dynamics, China Earthquake Administration, where this work was finalized. We thank editors and reviewers for their thorough, thoughtful reviews.

References

Argus, D. F., & Gordon, R. G. (1991). No-net-rotation model of current plate velocities incorporating plate motion model Nuvel-1. *Geophysical Research Letters*, *18*(11), 2039–2042. https://doi.org/10.1029/91GL01532

Berryman, K. R., Cochran, U. A., Clark, K. J., Biasi, G. P., Langridge, R. M., & Villamor, P. (2012). Major earthquakes occur regularly on an isolated plate boundary fault. *Science*, *336*(6089), 1690–1693. https://doi.org/10.1126/science.1218959

Bull, W. B. (1996). Prehistorical earthquakes on the Alpine fault, New Zealand. *Journal of Geophysical Research*, *101*(B3), 6037–6050. https://doi.org/10.1029/95JB03062

Cesca, S., Zhang, Y., Mouslopoulou, V., Wang, R., Saul, J., Savage, M., et al. (2017). Complex rupture process of the Mw 7.8, 2016, Kaikoura earthquake, New Zealand, and its aftershock sequence. *Earth and Planetary Science Letters*, *478*, 110–120. https://doi.org/10.1016/j.epsl.2017.08.024

Clark, K. J., Nissen, E. K., Howarth, J. D., Hamling, I. J., Mountjoy, J. J., Ries, W. F., et al. (2017). Highly variable coastal deformation in the 2016 M_W7.8 Kaikōura earthquake reflects rupture complexity along a transpressional plate boundary. *Earth and Planetary Science Letters*, *474*, 334–344. https://doi.org/10.1016/j.epsl.2017.06.048

Fialko, Y., Sandwell, D., Simons, M., & Rosen, P. (2005). Three-dimensional deformation caused by the Bam, Iran, earthquake and the origin of shallow slip deficit. *Nature*, *435*(7040), 295–299. https://www.ncbi.nlm.nih.gov/pubmed/15902247, https://doi.org/10.1038/nature03425

Green, R. G., White, R. S., & Greenfield, T. (2013). Motion in the North Iceland volcanic rift zone accommodated by bookshelf faulting. *Nature Geoscience*, *7*(1), 29–33.

Hall, L. S., Lamb, S. H., & Mac Niocaill, C. (2004). Cenozoic distributed rotational deformation, South Island, New Zealand. *Tectonics*, *23*, TC2002. https://doi.org/10.1029/2002TC001421

Hamling, I. J., Hreinsdottir, S., Clark, K., Elliott, J., Liang, C. R., Fielding, E., et al. (2017). Complex multifault rupture during the 2016 M-w 7.8 Kaikoura earthquake, New Zealand. *Science*, *356*, eaam7194. https://doi.org/10.1126/science.aam7194

Hill, E. M., Yue, H., Barbot, S., Lay, T., Tapponnier, P., Hermawan, I., et al. (2015). The 2012 Mw 8.6 Wharton Basin sequence: A cascade of great earthquakes generated by near-orthogonal, young, oceanic mantle faults. *Journal of Geophysical Research: Solid Earth*, *120*, 3723–3747. https://doi.org/10.1002/2014JB011703

Horst, A. J., Karson, J. A., & Varga, R. J. (2018). Large rotations of crustal blocks in the Tjörnes Fracture Zone of Northern Iceland. *Tectonics*, *37*, 1607–1625. https://doi.org/10.1002/2016TC004371

Jiao, L. Q., Tapponnier, P., Costa, F., Donze, F. V., Scholtes, L., Taisne, B., & Wei, S. J. (2018). Necking and fracking may explain stationary seismicity and full degassing in volcanic silicic spine extrusion. *Earth and Planetary Science Letters*, *503*, 47–57. https://doi.org/10.1016/j.epsl.2018.09.023

King, G., Klinger, Y., Bowman, D. & Tapponnier, P. (2005). Slip-partitioned surface breaks for the Mw 7.8 2001 Kokoxili Earthquake, China. *Bulletin of the Seismological Society of America*, *95*(2), 731–738, https://doi.org/10.1785/0120040101

Klinger, Y., Xu, X., Tapponnier, P., Van der Woerd, J., Lasserre, C., & King, G. (2005). High-resolution satellite imagery mapping of the surface rupture and slip distribution of the Mw 7.8, 14 November 2001 Kokoxili Earthquake, Kunlun Fault, Northern Tibet, China. *Bulletin of the Seismological Society of America*, *95*(5), 1970–1987. https://doi.org/10.1785/0120040233

Lamb, S. (2011). Cenozoic tectonic evolution of the New Zealand plate-boundary zone: A paleomagnetic perspective. *Tectonophysics*, *509*(3–4), 135–164. https://doi.org/10.1016/j.tecto.2011.06.005

Lamb, S., Arnold, R., & Moore, J. D. P. (2018). Locking on a megathrust as a cause of distributed faulting and fault-jumping earthquakes. *Nature Geoscience*, *11*(11), 871–875. https://doi.org/10.1038/s41561-018-0230-5

Langridge, R., Campbell, J., Hill, N., Pere, V., Pope, J., Pettinga, J., et al. (2003). Paleoseismology and slip rate of the Conway Segment of the Hope Fault at Greenburn Stream, South Island, New Zealand. *Annals of Geophysics*, *46*(5), 1119–1139. https://doi.org/10.4401/AG-3449

Litchfield, N. J., Van Dissen, R., Sutherland, R., Barnes, P. M., Cox, S. C., Norris, R., et al. (2013). A model of active faulting in New Zealand. *New Zealand Journal of Geology and Geophysics*, *57*(1), 32–56. https://doi.org/10.1080/00288306.2013.854256

Little, T. A., & Jones, A. (1998). Seven million years of strike-slip and related off-fault deformation, northeastern Marlborough fault system, South Island, New Zealand. *Tectonics*, *17*(2), 285–302. https://doi.org/10.1029/97TC03148

Little, T. A., Van Dissen, R., Kearse, J., Norton, K., Benson, A., & Wang, N. (2018). Kekerengu fault, New Zealand: Timing and size of Late Holocene surface ruptures. *Bulletin of the Seismological Society of America*, *108*(3B), 1556–1572. https://doi.org/10.1785/0120170152

Manighetti, I., Perrin, C., Dominguez, S., Garambois, S., Gaudemer, Y., Malavieille, J., et al. (2015). Recovering paleoearthquake slip record in a highly dynamic alluvial and tectonic region (Hope Fault, New Zealand) from airborne lidar. *Journal of Geophysical Research: Solid Earth*, *120*, 4484–4509. https://doi.org/10.1002/2014JB011787

Manighetti, I., Tapponnier, P., Gillot, P. Y., Jacques, E., Courtillot, V., Armijo, R., et al. (1998). Propagation of rifting along the Arabia-Somalia plate boundary: Into Afar. *Journal of Geophysical Research*, *103*(B3), 4947–4974. https://doi.org/10.1029/97JB02758

Mason, D. P. M., Little, T. A., & Van Dissen, R. J. (2006). Rates of active faulting during late Quaternary fluvial terrace formation at Saxton River, Awatere Fault, New Zealand. *Geological Society of America Bulletin*, *118*(11–12), 1431–1446. https://doi.org/10.1130/B25961.1

Morishita, Y., Kobayashi, T., Fujiwara, S., & Yarai, H. (2017). Complex crustal deformation of the 2016 Kaikoura, New Zealand, earthquake revealed by ALOS-2. *Bulletin of the Seismological Society of America*, *107*(6), 2676–2686. https://doi.org/10.1785/0120170143

Naar, D. F., & Hey, R. N. (1991). Tectonic evolution of the Easter microplate. *Journal of Geophysical Research*, *96*(B5), 7961–7993. https://doi.org/10.1029/90JB02398

Nicol, A., Khajavi, N., Pettinga, J. R., Fenton, C., Stahl, T., Bannister, S., et al. (2018). Preliminary geometry, displacement, and kinematics of fault ruptures in the Epicentral region of the 2016 Mw 7.8 Kaikōura, New Zealand, earthquake. *Bulletin of the Seismological Society of America*, *108*(3B), 1521–1539. https://doi.org/10.1785/0120170329

Perrin, C., Manighetti, I., Ampuero, J. P., Cappa, F., & Gaudemer, Y. (2016). Location of largest earthquake slip and fast rupture controlled by along-strike change in fault structural maturity due to fault growth. *Journal of Geophysical Research: Solid Earth*, *121*, 3666–3685. https://doi.org/10.1002/2015JB012671

Randall, K., Lamb, S., & Niocaill, C. M. (2011). Large tectonic rotations in a wide zone of Neogene distributed dextral shear, northeastern South Island, New Zealand. *Tectonophysics*, *509*(3–4), 165–180. https://doi.org/10.1016/j.tecto.2011.05.006

Rattenbury, M. S., Townsend, D., & Johnston, M. R. (compilers) (2006). *Geology of the Kaikoura area: Scale 1:250,000 geological map. Lower Hutt: GNS Science. Institute of Geological & Nuclear Sciences 1:250,000 geological map 13* (pp. 1–70). Retrieved from https://www.gns.cri.nz/Home/Our-Science/Land-and-Marine-Geoscience/Regional-Geology/Geological-Maps/1-250-000-Geological-Map-of-New-Zealand-QMAP/Digital-Data-and-Downloads

Scholtes, L., & Donze, F. V. (2013). A DEM model for soft and hard rocks: Role of grain interlocking on strength. *Journal of the Mechanics and Physics of Solids*, *61*(2), 352–369. https://doi.org/10.1016/j.jmps.2012.10.005

Segall, P. (2010). *Earthquake and volcano deformation*. USA: Princeton University Press.

Shi, X., Tapponnier, P., Wang, T., Wei, S., Wang, Y., Wang, X., & Jiao, L. (2019). Triple junction kinematics accounts for the 2016 Mw 7.8 Kaikoura earthquake rupture complexity. *Proceedings of the National Academy of Sciences of the United States of America*, *116*(52), 26,367–26,375. https://doi.org/10.1073/pnas.1916770116

Singh, S. C., Hananto, N., Qin, Y. F., Leclerc, F., Avianto, P., Tapponnier, P. E., et al. (2017). The discovery of a conjugate system of faults in the Wharton Basin intraplate deformation zone. *Science Advances*, *3*, e1601689. https://doi.org/10.1126/sciadv.1601689

Stirling, M. W., Litchfield, N. J., Villamor, P., Van Dissen, R. J., Nicol, A., Pettinga, J., et al. (2017). The M(W)7.8 2016 Kaikoura earthquake: Surface fault rupture and seismic hazard context. *Bulletin of the New Zealand Society for Earthquake Engineering*, *50*(2), 73–84. <Go to ISI>://WOS:000407278300002

Tapponnier, P., Armijo, R., Manighetti, I., & Courtillot, V. (1990). Bookshelf faulting and horizontal block rotations between overlapping rifts in southern Afar. *Geophysical Research Letters*, *17*(1), 1–4.

Thatcher, W. (2009). How the continents deform: The evidence from tectonic geodesy. *Annual Review of Earth and Planetary Sciences*, *37*(1), 237–262.

Vandissen, R., & Yeats, R. S. (1991). Hope Fault, Jordan thrust, and uplift of the seaward Kaikoura range, New-Zealand. *Geology*, *19*(4), 393–396.

Wallace, L. M. (2004). Subduction zone coupling and tectonic block rotations in the North Island, New Zealand. *Journal of Geophysical Research*, *109*, B12406. https://doi.org/10.1029/2004JB003241

Wallace, L. M., Barnes, P., Beavan, J., Van Dissen, R., Litchfield, N., Mountjoy, J., et al. (2012). The kinematics of a transition from subduction to strike-slip: An example from the Central New Zealand plate boundary. *Journal of Geophysical Research*, *117*, B02405. https://doi.org/10.1029/2011JB008640

Wang, T., Wei, S., Shi, X., Qiu, Q., Li, L., Peng, D., et al. (2018). The 2016 Kaikōura earthquake: Simultaneous rupture of the subduction interface and overlying faults. *Earth and Planetary Science Letters*, *482*, 44–51. https://doi.org/10.1016/j.epsl.2017.10.056

Wannamaker, P. E., Caldwell, T. G., Jiracek, G. R., Maris, V., Hill, G. J., Ogawa, Y., et al. (2009). Fluid and deformation regime of an advancing subduction system at Marlborough, New Zealand. *Nature*, *460*(7256), 733–736. https://www.ncbi.nlm.nih.gov/pubmed/19661914, https://doi.org/10.1038/nature08204

Xu, W., Feng, G., Meng, L., Zhang, A., Ampuero, J. P., Bürgmann, R., & Fang, L. (2018). Transpressional rupture cascade of the 2016 Mw 7.8 Kaikoura earthquake, New Zealand. *Journal of Geophysical Research: Solid Earth*, *123*, 2396–2409. https://doi.org/10.1002/2017JB015168

Xu, X., Tong, X., Sandwell, D. T., Milliner, C. W. D., Dolan, J. F., Hollingsworth, J., et al. (2016). Refining the shallow slip deficit. *Geophysical Journal International*, *204*(3), 1843–1862. https://doi.org/10.1093/gji/ggv563

Zachariasen, J., Berryman, K., Langridge, R., Prentice, C., Rymer, M., Stirling, M., & Villamor, P. (2006). Timing of late Holocene surface rupture of the Wairau Fault, Marlborough, New Zealand. *New Zealand Journal of Geology and Geophysics*, *49*(1), 159–174.

Zinke, R., Hollingsworth, J., Dolan, J. F., & Van Dissen, R. (2019). Three-dimensional surface deformation in the 2016 MW 7.8 Kaikōura, New Zealand, earthquake from optical image correlation: Implications for strain localization and long-term evolution of the Pacific-Australian plate boundary. *Geochemistry, Geophysics, Geosystems*, *20*, 1609–1628. https://doi.org/10.1029/2018GC007951